

Chapter 6

Experimental studies of equilibrium vortex properties in a Bose-condensed gas [1]

6.1 Introduction

After the initial observations of vortex lattices in Bose-Einstein condensed gases [22, 24, 25, 23], most of the experimental work has focused on dynamical behavior of vortices and lattices, including Kelvons [77, 95, 96], Tkachenko waves [28, 84, 29, 83, 31, 85, 33, 86, 32], and various nonequilibrium effects [71, 76]. Equilibrium properties, in contrast, have been relatively neglected by experimenters. This imbalance is not indicative of a lack of interesting physics in equilibrium behavior, but simply reflects the usual experimentalist's preference for measuring spectra rather than static structure. Theorists, on the other hand, have investigated equilibrium properties extensively [36, 44, 45, 94, 46, 35, 89, 97, 98, 41, 42, 99, 19], and our purpose in this chapter is to partially redress this imbalance with a series of experimental studies focusing on equilibrium properties of rotating condensates.

The vortex lattice in a rotating Bose-condensed gas naturally organizes into a regular triangular lattice, or Abrikosov lattice, originally observed in superconductors. The lattice can be well characterized by the nearest-neighbor lattice spacing and by the radius of each vortex core (b and r_v , respectively). The nearest-neighbor lattice spacing, b , is generally thought to be determined only by the rotation rate when in the high-rotation regime where the rotating BEC exhibits nearly rigid-body behavior. Nu-

merical work [45] and early analytical work [28], however, suggests that this rigid-body assumption yields lattice constants that are smaller than would be seen in the case of a finite-size trapped BEC. Recent work by Sheehy and Radzihovsky [44] has tackled this discrepancy analytically and found it to be a necessary consequence of the inhomogeneous density profile of the condensate. With this theory they address the question of why the lattice is so remarkably regular given the condensate density profile. They also derive a small, position-dependent, inhomogeneity-induced correction term to the lattice spacing. An interesting implication of this theory is that the vortices must move slightly faster than the surrounding superfluid even near the rigid-body limit. More striking still is the prediction that the superfluid should exhibit a radially-dependant angular velocity (or radial shear flow), which directly follows from their calculation of inhomogeneous vortex density. While a differential rotation rate is not directly observable in our system, the position-dependent variation of the nearest-neighbor lattice spacing is studied in §6.2. It should also be noted that the inhomogeneity in the areal density of vortices, predicted in Ref. [44], can also be derived in the limit of the lowest Landau level (LLL). This property of the LLL was first brought to our attention by A.H. MacDonald and has been the subject of two recent publications by Watanabe **et al.** [41] and Cooper **et al.** [42].

The second effect we study in this chapter concerns the core size of the vortices. Once rotation rate and density are fixed, the vortex core size is a length scale that the condensate chooses on its own. In this sense vortex core size constitutes a fundamental property of the system and has therefore been the subject of much theoretical work [94, 97, 98]. By analogy to superfluid ^4He , the core size is dictated by the atomic interactions and is of order of the healing length. For our system the healing length is only one and a half times the average interatomic spacing. As a result of this diluteness one might wonder if there are certain regimes of sufficiently low or high density where one would see a deviation from mean-field theory. Investigation of core size makes up §6.3.

Finally in §6.4 we examine the proposal that a measurement of the contrast of vortex cores could serve as a sensitive thermometer for a condensate in the regime for which the temperature is less than the chemical potential and other methods of thermometry become unreliable. We discuss our preliminary efforts to realize this vision. We are able to see an effect, but we have not yet been able to extend this measurement technique below the usual limits.

Note that our original paper on equilibrium effects [100] also contained a section examining the rotational suppression of quantum degeneracy. A description of this effect can be found in the thesis of Paul Haljan [54] or in [100].

6.2 The lattice constant

At first sight, vortex lattices, such as the one seen in figure 2.8(b), appear perfectly regular. However as noted in the introduction, Sheehy and Radzihovsky [44] predict that there should exist a small correction to the vortex density in the condensate due to the condensate, density inhomogeneity. One result from Ref. [44] is that the areal density of vortices is

$$n_v(\rho) = \frac{\Omega m}{\pi \hbar} - \frac{1}{2\pi R_\rho^2 (1 - (\rho/R_\rho)^2)^2} \ln[\hbar/(2.718 m\Omega\xi^2)] , \quad (6.1)$$

where m is the mass of rubidium and ξ is the healing length (calculated from the measured density). This equation can conveniently be thought of as the rigid body rotation (first term) plus the density inhomogeneity correction that reduces vortex density. We compare to experimental measurements by converting vortex density to a nearest-neighbor lattice spacing, conveniently expressed in units of condensate radius

$$b(\rho) = \sqrt{2/(3^{1/2}n_v(\rho))} \frac{1}{R_\rho} . \quad (6.2)$$

To study this lattice inhomogeneity effect experimentally, we generate condensates with rotation rates between $\Omega/\omega_\rho = 0.5$ and 0.9 . To extract the vortex separation,

we expand the cloud by a factor of 10 in the radial direction using the anti-trapped expansion technique. The condensate and vortices are fit as described in §2.3. The nearest-neighbor separation for a given vortex is measured by averaging the distance from the vortex center to the centers of the six nearest vortices. Due to low signal, vortices further than $0.9 R_\rho$ from the condensate center are disregarded. Any remaining vortex with fewer than six nearest neighbors (i.e., a vortex in the outer ring) is used as a neighbor to other vortices but is not itself included in the final data. Obviously using the six nearest neighbors assumes a triangular lattice structure, so before fitting, each image is checked for defects in the lattice. Any image exhibiting broken lattice planes is not considered. Once the nearest-neighbor separation is measured, it is normalized by the expanded condensate radius to compare to equation 6.2. For this comparison, R_ρ , Ω , and ξ are measured or calculated from an in-trap image. To improve the theory fit, we allowed R_ρ to float, but, in each case, the fit value for R_ρ was within 5% of the measured value. Noise is suppressed by binning the lattice-spacing data by radial displacement of the vortex from the center.

Figure 6.1 shows a comparison to theory for three physical condensates and one numerically generated condensate density profile. Figure 6.1(a) is data taken from the condensate in figure 2.8(a). The two points shown correspond to the measured vortex density for the center vortex (first point) and the average vortex density for the first ring of vortices. Also plotted is equation 6.2 (solid line) and the expected nearest-neighbor lattice spacing for rigid body rotation (dashed line). The imperfect fit may be partly due to the discrete nature of the data, vis-a-vis a continuum theory [44]. Plots (b) and (c) are condensates with increasing rotation rates where (c) is taken from image 2.8(b). Plot (d) is a comparison with numerical data prepared with parameters similar to the experimental situation in (c). Figure 6.1(e) is the same data in figure 6.1(c) but plotted without the suppressed zero to emphasize the smallness of the position dependant effect. The areal density of vortices is constant to 2% over a region that experiences an atom-

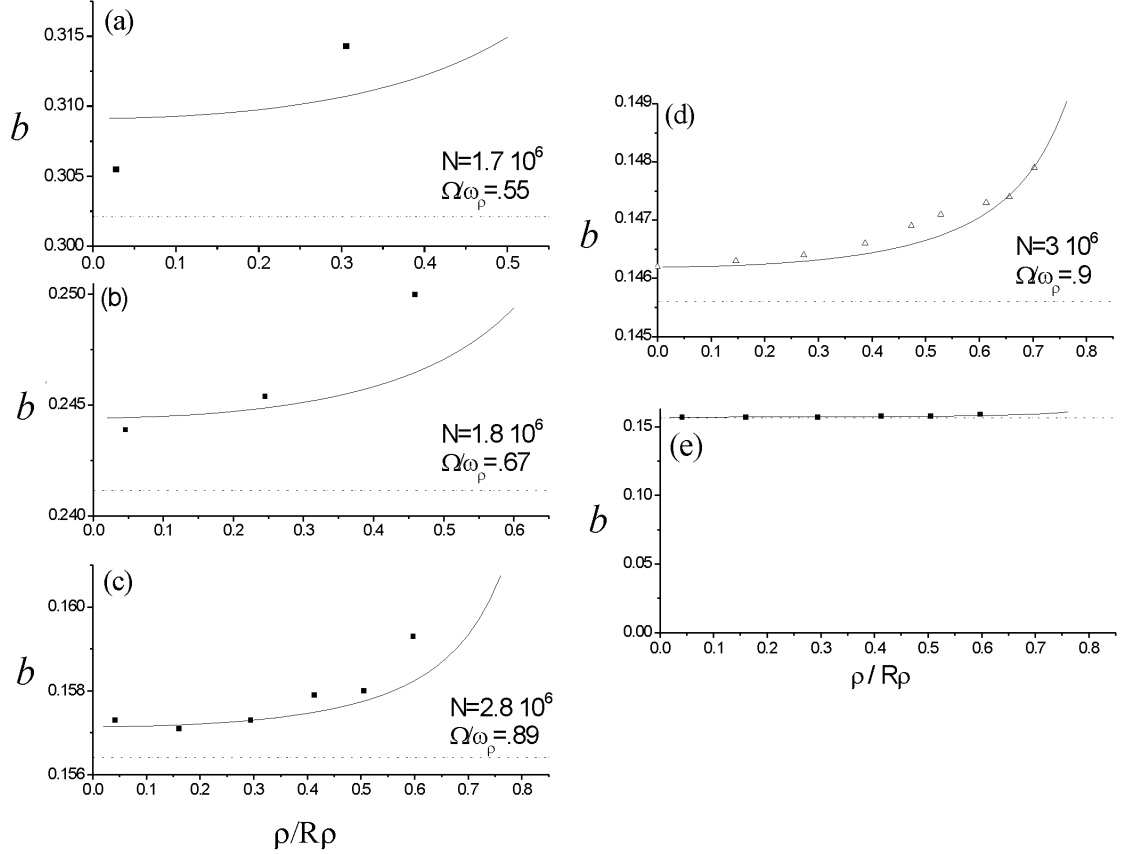


Figure 6.1: Measured and binned lattice spacings as a function of radial position ρ . The solid curve is the theory result (equation (6.2)) of Sheehy and Radzihovsky [44]. The rigid-body-rotation lattice spacing is also plotted for comparison (dashed line). Plots (a-c) are experimental data with increasing rotation. Plot (a) and (c) are data taken from the condensate in Figs. 2.8(a) and (b), respectively. Plot (d) is the same effect observed in the numerical data. One can see that theory and experiment show a similar dependence on radial position and that the fractional amplitude of the density inhomogeneity effect is suppressed at higher rotation. Plot (e) is the data in (c) plotted without suppressing the zero. The vortex lattice spacing changes less than 2% over a region in which the atom density varies by 35%.

density variation of 35%.

6.3 Vortex core size

The other defining length scale of the vortex lattice is the core radius. Here we study the core radius in the Thomas-Fermi regime (as opposed to the lowest Landau level regime, described later) where it should scale with the healing length. A theoretical value for the vortex core radius was generated by performing a numerical simulation for a 3D BEC containing an isolated vortex and comparing the fitted radius of this vortex to the corresponding healing length. Fitting the simulation in the same manner that we later treat the experimental data (described in §2.3) we obtain an expression for the core radius of

$$r_v = 1.94 \times \xi , \quad (6.3)$$

with healing length $\xi = (8\pi n a_{sc})^{-1/2}$, where a_{sc} is the scattering length and n is the density-weighted atom density. For the data presented, n is determined from the in-trap image before expansion.

Core size measurements and fractional core area (discussed in the next subsection) measurements require considerable attention to detail. In pursuing these measurements, we find that nearly everything — from focusing issues, to lensing due to off resonant imaging light, to even imperfect atom transfer into the anti-trapped state before expansion — can lead to an overestimation of the vortex core size. By far the biggest potential systematic error in our system is axial expansion, which, as noted in §2.3, requires careful attention.

A range of core sizes is achieved by varying the initial number of atoms loaded into the magnetic trap prior to evaporation. To avoid the core size saturation effect, due to high condensate rotation [36], we consider only clouds with $\Gamma_{LLL} > 10$, where $\Gamma_{LLL} \equiv \mu / (2\hbar\Omega)$ is the LLL parameter and μ is the chemical potential. This ratio of

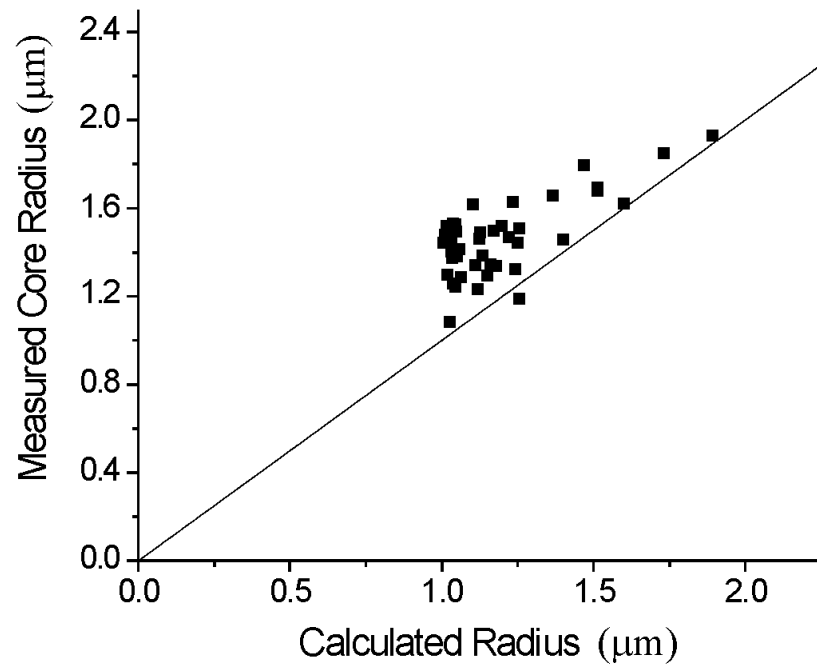


Figure 6.2: Comparison of measured core radii with the Thomas-Fermi prediction (equation (6.3)) represented by the solid line. Black squares are the core size in expansion scaled by the radial expansion of the condensate so that they correspond to the in-trap values. Data shows reasonable agreement with theory. The fact that the measured core size is consistently larger is likely due to the fact that nearly all our imaging systematics lead to an overestimation of the vortex core size.

chemical potential to rotational energy approaches unity as we enter the LLL regime, while at values of 10 or greater we should be firmly in the Thomas-Fermi regime. In practice this requires only that we keep the condensate rotation rate low. Core size is measured by fitting the expanded image with a Thomas-Fermi profile and each core with a 2D Gaussian. For figure 6.2 the measured core radius in expansion is scaled back to the corresponding in-trap value using the radial expansion factor discussed in §2.3. To reduce scatter we consider only vortices located less than half a condensate radius out from the center. Additionally we find that some vortices appear to have some excitation or bending which leads to a poor fit. To filter these out we consider only vortices that have a contrast greater than 0.6. Here contrast is defined, with respect to the integrated (along the line of sight) condensate profile, as the peak of the “missing” column density at the vortex position divided by the smoothed Thomas-Fermi profile at the same position.

From figure 6.2 we can see that the data and the Thomas-Fermi theory agree reasonably well. The data do seem to be slightly above the theory value, but we are hesitant to make too much of this because, as noted before, there are many systematic errors that tend to bias the data toward larger core size. Measurement is easier and the agreement better, on the low density, large-core side of the graph.

At an early stage in this work, we speculated that the mean-field Gross-Pitaevskii equation might not give a good quantitative description of vortex core size because the core size is particularly sensitive to the healing length ξ . At our highest densities, while the gas is nominally dilute ($na_{sc}^3 < 10^{-5}$, where a_{sc} is the interatomic scattering length), the mean interatomic distance $n^{-1/3}$ is only a factor of 1.5 less than ξ . Our data, however, do not support this hypothesis. The roughly 25% discrepancy between our measurements and the mean-field prediction shown in figure 6.2 is comparable to possible systematic errors in our measurements of the smaller cores that exist at high densities. In retrospect, our experimental design is such that we are unlikely to be able

to see a mean-field failure even if one were to exist. During the radial expansion, the density drops. Thus the accuracy of the mean-field approximation is likely to improve significantly during the expansion. Our anti-trapped expansion, while more rapid than a conventional ballistic expansion, is still slow compared to the rate at which a vortex can adiabatically relax its radius [36] (approximately μ/\hbar). Any non-mean-field corrections to the vortex core size will likely relax away before the cores have expanded to be large enough for us to reliably image them.

6.4 Core contrast and condensate temperature

Since the very first observations of dilute-gas BEC, the temperature of the sample has been determined by imaging the “skirt” of thermal atoms that extends beyond the radius of the condensate. In practice, it is difficult to extend this measurement below about $T/T_c = 0.4$, except in very special cases (for instance when a Feshbach resonance is used to set the scattering length to zero). For low temperatures, the density of thermal atoms becomes so low that they are difficult to image. Moreover, when the temperature becomes lower than or comparable to the chemical potential of the self-interacting condensate, the spatial extent of the thermal cloud is no longer appreciably larger than the condensate itself.

It was suggested that vortex cores might serve as “thermal-atom concentration pits”, in order to enhance thermometry at low temperatures. In a simple Hartree-Fock (HF) picture of the interaction between thermal atoms and the condensate, the condensate density represents a repulsive interaction potential to the thermal atoms. Along the nodal line of a vortex core, the condensate density and presumably its repulsive interaction potential vanish. Thus, the thermal atoms would experience the lowest combined interaction and magnetic potential within the cores of vortices. As a result, their density would be highest there. Additionally, images of thermal atoms in the vortex core could be taken against a vanishing background condensate density. Moving

beyond the HF approximation, one finds a more complicated picture. The Bogoliubov spectrum of very long wave-length thermal phonons extends all the way down to the chemical potential. One should contrast this energy with the energy of a thermal atom confined to a vortex core. Perhaps the atom experiences no interaction energy. However, the kinetic energy cost of bending its wave function to fit inside a core with a radius of the order of healing length must, by definition, be comparable to the chemical potential. In the limit of very elongated vortex cores, there can be very low-energy, core-bending modes [77, 101]. Thermal excitations of these modes would manifest as a temperature-dependent contrast ratio. We expect this effect is unlikely to be important in the relatively flattened geometry of our highly rotating condensates. In any case, without more rigorous analysis, it is not easy to predict how the contrast ratio of our vortices should vary with temperature, but we nonetheless set out to do a preliminary study of the effect.

We vary the final condensate temperature by changing our rf-evaporation end point. This produces a cloud with temperatures between $5 - 50$ nK or T/T_c between 1 and less than 0.4. Here T_c is calculated from the trap frequencies and a measurement of total atom number using the formula $T_c = 0.94\hbar\tilde{\omega}_{ho}N^{1/3}$, where $\tilde{\omega}_{ho}$ has been adjusted for rotation according to the equation $\tilde{\omega}_{ho} = \omega_{ho}(1 - \Omega^2/\omega_\rho^2)^{1/3}$. When possible, T is extracted from a two-component fit to the in-trap image. Because our rotation rate and temperature are linked through the 1D evaporative process, it is unavoidable that Ω also varies during the data set.

To measure core contrast, we expand the cloud using the usual expansion procedure. The atom cloud is expanded radially by a factor of 13 to ensure that the cores are large compared to our imaging resolution. However, because we no longer care about the precise core size we do not suppress the axial expansion. Additionally, the axial expansion actually reduces background fluctuations in the measured core contrast. With a factor of two axial expansion, cores become much rounder and clearer as shown

in figure 2.8(c). These changes allow us to achieve a higher core contrast and quieter signal than we can without expansion.

The term core brightness (1-contrast ratio) will be our metric for this experiment. We define core brightness (\mathcal{B}) as $n_{2D}(core)/n_{2D}(cloud)$, where $n_{2D}(core)$ is the observed atom density, integrated along the line of sight, at the core center, and $n_{2D}(cloud)$ is the projected integrated atom density at the same point, based on a smoothed fit to the overall atom cloud. To determine $n_{2D}(cloud)$, we fit the condensate image to a Thomas-Fermi profile and the surrounding thermal atoms to a Bose distribution. We find $n_{2D}(core)$ by fitting each vortex with a Gaussian to determine its center and then averaging five pixels around the center point to determine the integrated density. Brightness is calculated for each vortex and then averaged with other vortices in the cloud. To suppress noise from low signal, vortices further than $0.4 R_\rho$ from the condensate center are disregarded for this measurement. The $n_{2D}(core)$ term necessarily contains signal from the surrounding thermal atoms because the vortices do not penetrate the thermal component. Thus, one expects to see a steady decrease in \mathcal{B} with decreasing temperature, as atoms not necessarily in the vortex core, but still in the integrated line of sight, disappear. One would hope that \mathcal{B} continues to decrease even for T/T_c below 0.4 for this analysis to be a viable means of extending condensate thermometry.

We are in the awkward position of comparing our core contrast measurement to a temperature measurement that, as previously described, is expected to fail at low temperatures. To monitor this failure, we calculate a simplistic core brightness (\mathcal{B}_{simple}) by comparing the fitted in-trap condensate and thermal cloud profiles. Here $\mathcal{B}_{simple} \equiv \tilde{n}_{2D}(thermal)/(\tilde{n}_{2D}(condensate) + \tilde{n}_{2D}(thermal))$ where $\tilde{n}_{2D}(condensate)$ and $\tilde{n}_{2D}(thermal)$ are the smoothed condensate and thermal cloud profiles integrated along the z-axis and averaged over a region of radius less than $0.4 R_\rho$ from the condensate center. The term \mathcal{B}_{simple} can be thought of as the core brightness one would expect based on the undoubtedly false assumption that the condensate and thermal atoms do

not interact. It is interesting to compare \mathcal{B} to \mathcal{B}_{simple} since this same dubious assumption is implicit in the standard thermometry technique of fitting the thermal “skirt”.

In figure 6.3, \mathcal{B} and \mathcal{B}_{simple} are plotted versus the final evaporative cut. For our experiment, the thermal cloud can be reliably fit for $T/T_c > 0.6$ and less reliably fit for $T/T_c > 0.4$. In both these regions T/T_c decreases continuously with lower final evaporative cut. It is assumed that for T/T_c just below 0.4, this trend continues. For reference, three values of T/T_c (measured from the thermal “skirt”) are included in the plot. One can see that \mathcal{B} does steadily decrease with lower temperature for $T/T_c > 0.4$. It is interesting to note that \mathcal{B}_{simple} closely tracks \mathcal{B} at the higher temperatures and then diverges from \mathcal{B} as the cloud gets colder. Presumably, this divergence occurs because thermal atoms are pushed away from the condensate center as interactions between the condensate and the thermal cloud become important. The fact that \mathcal{B}_{simple} diverges upwards is likely due to the tendency of our fitting technique to overestimate the thermal cloud density at high condensate fractions. The failure of \mathcal{B}_{simple} at low temperatures also throws into suspicion the quoted T/T_c since they are determined from the same two-component fit.

In contrast, as \mathcal{B}_{simple} begins to fail, \mathcal{B} continues its previous smooth downward trend. It is also interesting to note that at an rf of 2.35 MHz, we see a \mathcal{B} of 0.13-0.15, which is not that far off from the work of Virtanen **et al.** [98] who predict that atoms trapped in the core would lead to a \mathcal{B} of 0.1 at a T/T_c of 0.39. Unfortunately, our efforts to observe a \mathcal{B} of less than 0.125 have failed so far, as can be seen from the data points at 2.3 MHz in figure 6.3. This limit impedes our ability to measure temperatures colder than 0.4 T/T_c . Currently, it is unclear what the source of this limit is. Perhaps the same imaging systematics that make our vortex radius unreliable at the 10% level are also preventing us from seeing a core brightness level less than 0.13, or a very slight tilt of the vortices may occur during expansion.

As a caveat to the previous discussion, the same limitations that inhibit conden-

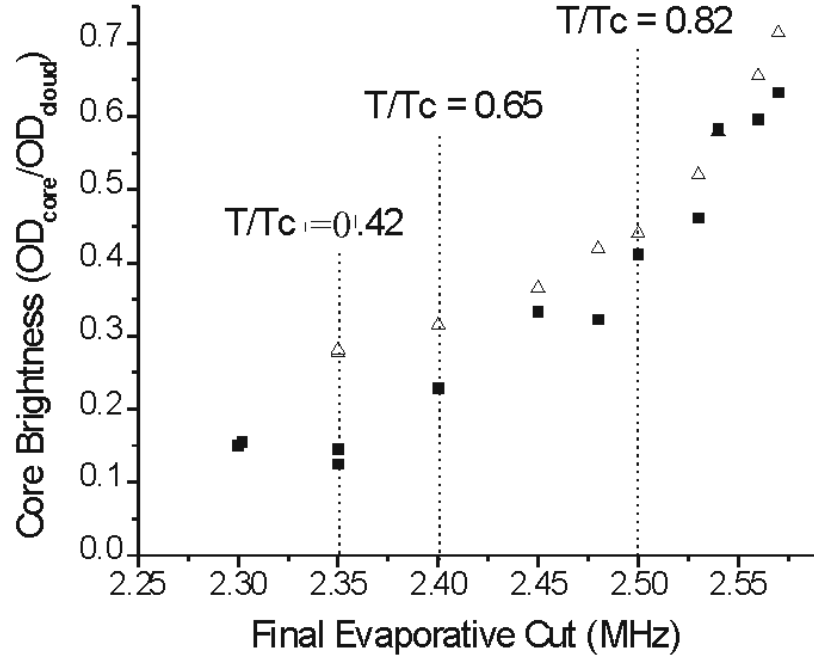


Figure 6.3: Measured core brightness as a function of final rf evaporative cut. Within our ability to measure, T/T_c decreases continuously with the rf frequency. For the black squares brightness (\mathcal{B}) is defined as the 2D atom density at the vortex core divided by the 2D atom density of the overall smoothed condensate plus thermal cloud profile at the same point. For the open triangles a simplistic brightness (\mathcal{B}_{simple}) is calculated from the ratio of the 2D atom density of the thermal cloud to the 2D atom density of the overall smoothed condensate and thermal cloud profile. At high temperatures \mathcal{B} and \mathcal{B}_{simple} exhibit a clear dependence on the final rf cut. At lower temperatures it is encouraging that as \mathcal{B}_{simple} begins to fail \mathcal{B} is still continuing a smooth trend downward. Disappointingly at very low temperatures, \mathcal{B} plateaus at about 0.14.

sate thermometry below T/T_c of 0.4 will also reduce the efficacy of evaporative cooling in the same regime. Additionally, the already inefficient 1D nature of our evaporation would exacerbate such a cooling problem. Perhaps the simplest explanation for the failure of \mathcal{B} to decrease with very deep rf cuts is that the condensate fraction is no longer increasing. One could imagine that our measured \mathcal{B} is faithfully following the temperature we achieve.

In summary, the conclusions of our preliminary attempt to extend thermometry with core brightness are encouraging but ambiguous. New ideas are needed before we can make further progress.